Collision Dynamics of Large Argon Clusters

Liu Ming, Nikola Marković, Marcus Svanberg, and Jan B. C. Pettersson*,†

Department of Chemistry, Physical Chemistry, Göteborg University, S-412 96 Göteborg, Sweden

Received: December 13, 1996; In Final Form: March 21, 1997[⊗]

Classical trajectory calculations of collisions between Ar_{1000} clusters are carried out to investigate the effects of relative velocity and impact parameter on energy transfer and dynamical behavior. In the velocity range 100−1000 m/s, we conclude that the outcome of the collisions can be classified into a few characteristic scattering channels. We observe coalescence, stretching separation, and shattering collisions, and each collision process dominates within distinguishable parameter ranges. A major part of the available energy ends up in vibrational degrees of freedom, and internally hot systems cool by evaporation as well as more severe fragmentation for high-energy collisions. High rotational excitation is observed for large impact parameter values, and the maximum rotational energy of the collision complex is concluded to mainly determine whether a collision will result in coalescence or stretching separation. The results are related to experimental data for collisions between large liquid droplets, and we conclude that argon clusters in the nanometer range partly resemble the larger systems. The boundary between coalescence and stretching separation is surprisingly well predicted by macroscopic models.

1. Introduction

Clusters have received considerable attention because of their intermediate position between free atoms or molecules and bulk material. Experimental and theoretical studies have been carried out to investigate the change of physical and chemical properties with cluster size, including cluster structure and reactivity, and the emergence of bulk and surface properties. In the same way, *collisions* between clusters constitute an intermediate case between molecular collisions and collisions between particles, or droplets, in the macroscopic state. In the present paper, we are interested in this transition from microscopic to macroscopic dynamics, and we address the following question; When does a cluster start to behave as a macroscopic particle or droplet? We present classical trajectory calculations for collisions between Ar clusters consisting of 1000 atoms (cluster diameter 4.5 nm) and investigate the effects of relative collision velocity and impact parameter on energy transfer and dynamical behavior. In the velocity range 100−1000 m/s, we observe coalescence, stretching separation, and shattering collisions, and the different types of collisions are found to dominate within distinguishable parameter ranges. Our results are compared with experimental data for collisions between water droplets in the micrometer range, and similarities and differences between the systems are identified. We show that theoretical models used to predict stretching separation for large water droplets also can describe collisions between Ar_{1000} clusters.

We know of two earlier studies where the collision dynamics of nanometer size particles was studied. Greenspan and Heath[1] carried out classical trajectory calculations of collisions between model clusters with a size of 2051 monomers. The individual molecules were modeled as single mass particles, and the molecule−molecule interaction was described by a potential of the form $A/r^4 - B/r^2$. Greenspan and Heath identified different modes that the colliding system could obtain and compared with observations for large droplets. A similar study using a more refined potential for the molecule−molecule interaction was carried out by Wyatt.[2] Other investigations of cluster−cluster collisions have mainly considered much smaller clusters. Schmidt et al.[3] carried out molecular dynamics calculations of collisions between Na_9 clusters. Schmidt et al.[4] also investigated the dynamics of $C_{60} - C_{60}^+$ collisions. Related studies have treated interactions between clusters and single molecules. Lewerenz et al.[5] studied "pickup" of molecules by large ($n > 10^3$) helium clusters. The adsorption of single molecules on large argon[6,7] and water[8] clusters has also been investigated. Cluster−surface collisions, which are closely related to cluster−cluster collisions, have recently been studied by Pettersson and co-workers,[9−13] Xu et al.,[14,15] Cleveland and Landman,[16] and Jortner and co-workers.[17,18]

When instead collisions between macroscopic droplets are considered, numerical methods such as the so-called immiscible lattice gas model[19] and the volume-of-fluid technique[20] have been used to simulate the incompressible Navier−Stokes equations for large liquid systems. We believe that the molecular dynamics approach used in the present study is a good alternative for investigations of collisions involving nanometer particles. In this size range, experimental investigations are difficult to perform, and the validity of numerical methods used for large droplets is not well-known. As will be seen below, the molecular dynamics method can also be used to test whether empirical models for collisions of micrometer objects are valid at a smaller scale. The present study is the first in a series of cluster−cluster investigations including more complicated systems such as molecular clusters and binary mixtures. A study of water cluster collisions is in progress.[21]

The paper is organized as follows: The calculation procedure is described in the next section. The results are collected in section 3 and discussed in section 4. The main conclusions from this study are finally given in section 5.

2. Model and Methods

2.1. Interaction Potential and Cluster Structure. The Ar−Ar interaction was described using a truncated and shifted Lennard-Jones potential,

* To whom correspondence should be addressed. E-mail janp@phc.chalmers.se.
† Also at the Division of Environmental Sciences, Göteborg University.
⊗ Abstract published in *Advance ACS Abstracts,* May 1, 1997.

S1089-5639(96)04060-1 CCC: $14.00

$$V(r) = \begin{cases} 4\epsilon[(\sigma/r)^{12} - (\sigma/r)^6] - 4\epsilon[(\sigma/r_c)^{12} - (\sigma/r_c)^6], & r \le r_c \\ 0, & r > r_c \end{cases} \quad (1)$$

with parameters $\epsilon = 10.3$ meV and $\sigma = 0.34$ nm.[22] A cutoff radius corresponding to 2.5σ was used, i.e., $r_c = 0.85$ nm.

The initial structure for the Ar_{1000} cluster was obtained by minimizing the potential energy for a close-packed sphere of 1000 Ar atoms using molecular dynamics and gradually scaling down the atomic velocities during the simulation until the internal temperature was below 10^{-4} K. The resulting cluster had a radius of 2.2 nm and a binding energy of 65.3 meV per atom. Using the untruncated potential a value of 73.1 meV was obtained, which is in good agreement with the result found in ref 23. The collision energy dependence obtained will be slightly shifted due to the lower binding energy for the truncated potential. Qualitative differences in the collision dynamics due to the truncation may occur for very low relative velocities but are not expected to influence the present results.

2.2. Trajectory Calculations. At the beginning of the trajectory one cluster was located at the origin of a Cartesian coordinate system. This *target* cluster was rotated using three randomly selected Euler angles but given no rotational or translational energy. Another randomly oriented cluster was located 6.3 nm away along the negative *y*-axis with an *x*-coordinate between 0 and 4 nm corresponding to the impact parameter, *b*. This *incident* cluster was given a velocity, v_{rel}, in the range 100−1000 m/s in the direction of the *y*-axis. Note that both clusters have identical structures, and the atoms were given no internal velocities. After a relaxation period of 0.4 ps the temperature stabilizes around $T \approx 3 \times 10^{-5}$ K.

The equations of motion were integrated by the velocity Verlet integrator[24] using a time step, Δt, of 20 fs for most of the calculations. For collisions classified as being of the shattering type (see section 2.3), a smaller time step, $\Delta t = 5$ fs, was used. The relative energy conservation error was less than 10^{-4} over a 200 ps integration period. The reliability of the computed quantities was checked by repeating some of the calculations using a shorter time step. A comparison showed that the dynamical behavior and computed properties obtained using $\Delta t = 20$ fs were very similar to the results obtained with $\Delta t = 1$ fs. Selected trajectories recalculated using a cutoff radius $r_c = 3.0\sigma$ did not significantly deviate from those computed with $r_c = 2.5\sigma$.

2.3. Data Analysis. The trajectories were propagated for 200 ps. Along the trajectory some interesting properties were calculated at certain time intervals, normally taken to be a few picoseconds or less. These properties were the vibrational temperature and the rotational energy of the two largest fragments. Two atoms were defined to belong to the same cluster fragment if their separation was less than the cutoff distance r_c.[25] Since any two argon atoms interacting were defined as being part of a cluster, this definition will include also very weakly bound systems. The rotational and vibrational energies, as well as the corresponding temperatures, were defined in the same way as previously.[9−12]

The instantaneous rotational energy of a cluster fragment with *N* atoms was obtained as

$$E_{rot} = {}^1/_2\boldsymbol{\omega}\cdot\mathbf{L} \quad (2)$$

where **L** is the angular momentum with respect to the center of mass of the fragment and $\boldsymbol{\omega}$ is the corresponding angular velocity.[26,27] The instantaneous rotational energy varies rather smoothly with time because the overall shape of the largest fragments usually do not change rapidly.

The vibrational kinetic temperature of a fragment was calculated using two independent methods. The first method is based on the equipartition theorem. In this case the temperature is obtained as

$$T_{vib} = 2E_{v,k}/(3N - 6)k_B \quad (3)$$

where $E_{v,k}$ is the instantaneous value of the kinetic part of the vibrational energy. The temperature obtained in this way is rather stable due to the large number of vibrational degrees of freedom. This quantity is, however, just a measure of energy in terms of temperature. To check whether the system was thermalized, we also analyzed the vibrational kinetic energy distribution $P(E_{v,k,i})$, where $E_{v,k,i}$ is the vibrational kinetic energy of the *i*th atom. It is obtained as follows

$$E_{v,k,i} = \frac{1}{2}m\left[\left(\frac{p_{x,i}}{m} - v_{rot,x,i}\right)^2 + \left(\frac{p_{y,i}}{m} - v_{rot,y,i}\right)^2 + \left(\frac{p_{z,i}}{m} - v_{rot,z,i}\right)^2\right] \quad (4)$$

where $v_{rot,i}$ is the rotational velocity of the *i*th atom. According to the canonical ensemble

$$P(E_{v,k,i}) \propto {E_{v,k,i}}^{1/2} \exp(-E_{v,k,i}/k_B T_{vib}) \quad (5)$$

The logarithm of $P(E_{v,k,i}){E_{v,k,i}}^{-1/2}$ is plotted versus $E_{v,k,i}$. Thus, if the distribution is thermal, a straight line with slope $-1/k_B T_{vib}$ is obtained. Strictly speaking, since there are no center-of-mass translational and rotational energies accounted for in the energy term $E_{v,k,i}$, the relation is only approximately valid. However, as there are $3N - 6$ vibrational degrees of freedom compared to six translational and rotational degrees of freedom, it is a very good approximation for our cluster sizes.

3. Results

Collisions between cold clusters consisting of 1000 argon atoms have been studied using molecular dynamics simulations. The relative translational velocity was chosen in the range from 100 to 1000 m/s in steps of 100 m/s, and the impact parameter was selected from 0 to 4 nm in steps of 0.5 nm. All trajectories were integrated for 200 ps.

3.1. Scattering Channels and Their General Features. *3.1.1. Coalescence Collisions.* When the relative translational velocity is low, coalescence collisions are mainly observed as illustrated in Figure 1a. The collision energy is completely transferred into internal vibrational and rotational motion. This type of collision is observed for the full range of impact parameters (0−4 nm) if v_{rel} is sufficiently low (less than 250 m/s). Significant mixing of atoms between the incident and target clusters on the time scale of a few hundred picoseconds is usually seen only for high collision energy due to the ultracold initial temperature of the clusters. For small impact parameters ($b < 1$ nm) and a relatively high v_{rel} (600−800 m/s), evaporation from the formed complex becomes important due to the high internal temperature of the cluster. The dynamical behavior is in this case very similar to the coalescence collisions without evaporation, except that some slight mixing is observed and some small fragments formed, such as monomers, dimers, or trimers. We classify the collision as coalescence if the largest surviving cluster consists of more than 1600 atoms and the second largest fragment of fewer than 25 atoms at the end of the trajectory.

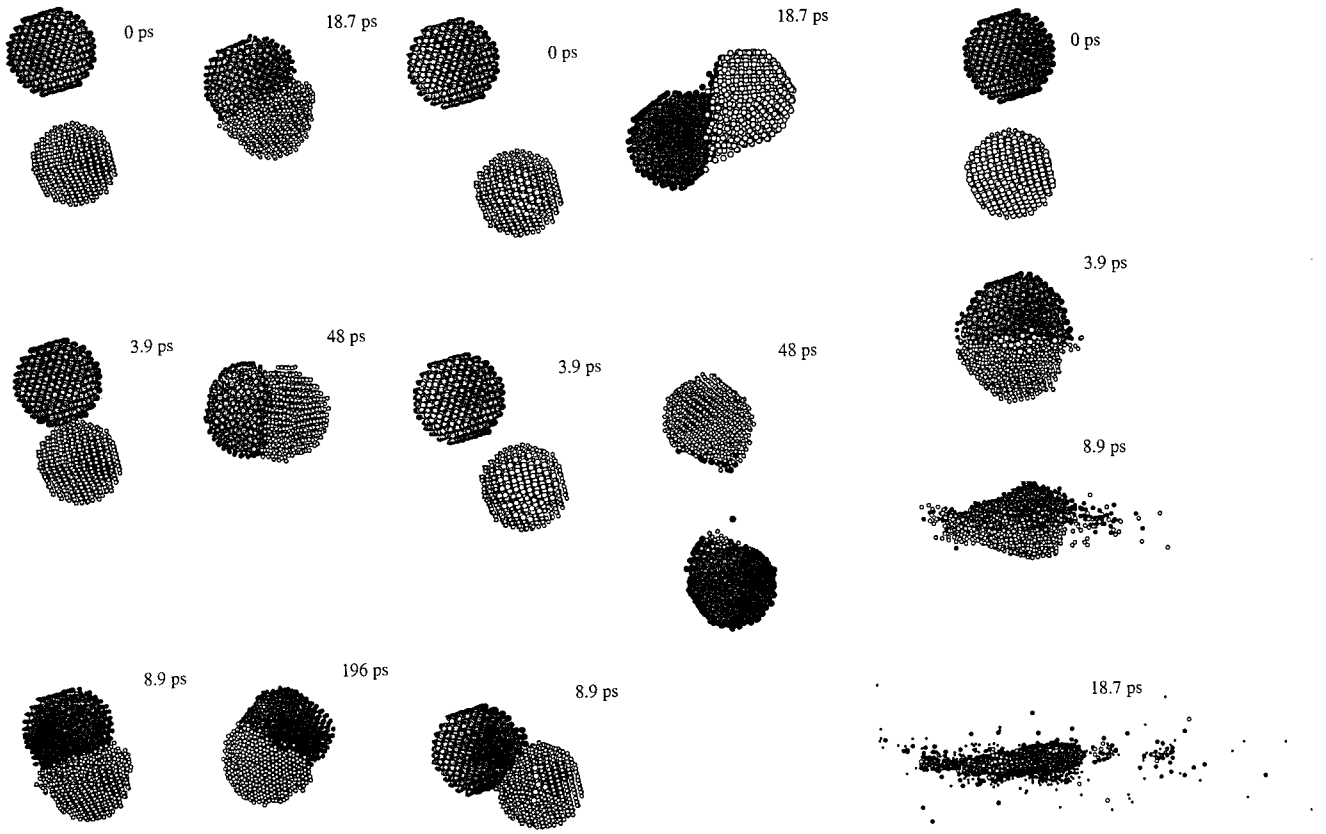

Figure 1. Illustration of different scattering channels for $Ar_{1000} + Ar_{1000}$ collision: (a, left) Coalescence: $v_{rel} = 400$ m/s and $b = 1$ nm. (b, middle) Stretching separation: $v_{rel} = 500$ m/s and $b = 3$ nm. (c, right) Shattering: $v_{rel} = 1000$ m/s and $b = 0$ nm.

3.1.2. Stretching Separation Collisions. Stretching separation collisions are observed when a high velocity is accompanied by a relatively large impact parameter value. This type of collision is illustrated in Figure 1b. After collision, the two largest fragments each contain between 700 and 1200 atoms. There is also a possibility for the formation of small fragments. The internal temperature is increased, but the rotational excitation dominates due to the large angular momentum involved. Additionally, some mass transfer is usually observed, and the degree of mass transfer increases with increasing relative velocity.

3.1.3. Shattering Collisions. Shattering collisions are only observed for velocities above 800 m/s combined with a impact parameter value less than 1.0 nm. This type of collision is illustrated in Figure 1c for $v_{rel} = 1000$ m/s and $b = 0$. Almost all collision energy is transferred into vibrational motion during a very short time interval at the beginning of impact. Therefore, the internal energy becomes too high to be released by a slow evaporation process. This leads to the formation of many small as well as moderately sized fragments during the collision. In the present calculations the largest fragment consists of fewer than 1600 atoms and the rest of the fragments of 1−699 atoms, with a very high probability for small fragments.

3.2. Energy Transfer Process. Since the clusters are initially cold, energy will be transferred from translational modes into vibrational and rotational ones. For a given collision energy, the fraction of energy transferred into rotation increases with increasing impact parameter as long as the collision is of the coalescence type. Nonetheless, since the number of vibrational degrees of freedom ($3N - 6$) is much larger than the number of rotational degrees of freedom (which are just three), the process is dominated by translational to vibrational energy transfer, except for cases with low collision energy and high impact parameter.

In this study, the kinetic temperature is employed to describe the vibrational kinetic energy per degree of freedom. This is a reasonable concept due to the large number of degrees of freedom. The vibrational temperature as a function of time for different types of collisions is presented in Figure 2a. The dynamical behavior of the vibrational excitation is similar for the different types of collisions. The temperature rises sharply at the beginning of impact and is followed by a relaxation process where the temperature is equilibrated around a quite stable value. From Figure 2a, as one would expect, the height of the impact peaks and the final temperatures are correlated with the initial relative translational energy. The time-resolved rotational energy of the largest fragment for the same trajectories are presented in Figure 2b. Note that the rotational energies are presented on a logarithmic scale. If the energy per degree of freedom is compared between the vibrational and rotational motion, the rotational energy transfer is much more active than the vibrational energy transfer. This is also typical for energy transfer taking place in molecule−molecule collisions[28−30] when the interaction potential is not particularly strong. One point should be borne in mind: presented vibrational kinetic temperature and rotational energy are only for the largest fragment, and the number of atoms may vary during the collisions as shown in Figure 2c. For instance, for the coalescence collision ($b = 1$ nm, $v_{rel} = 400$ m/s) the number of atoms in the largest fragment is constant, 2000; for the stretching separation collision ($b = 3$ nm, $v_{rel} = 500$ m/s), this number is changed from 2000 to 1030 after separation; for the shattering collision ($b = 0$, $v_{rel} = 1000$ m/s) the number of atoms in the largest fragment is gradually changed from 2000 to 1500. To check whether or not thermal equilibrium is reached for the vibrational kinetic energy, the atomic vibrational kinetic energy distributions at 190 ps are presented in Figure 3, which confirms that the internal temperature is in good agreement with the final temperature

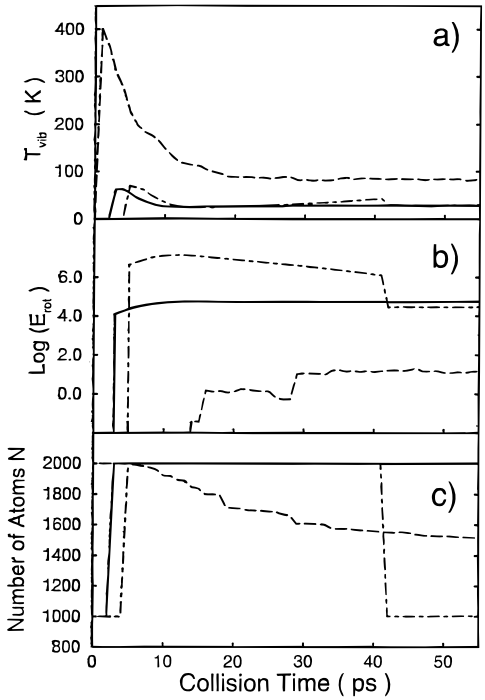

Figure 2. Time-resolved vibrational kinetic temperatures, rotational energies, and number of atoms in the largest fragment are presented for the three collisions shown in Figure 1. The solid lines represent the coalescence collision, the dot-dashed lines the stretching separation collision, and the dashed lines the shattering collision. (a) Vibrational kinetic temperature. (b) Logarithm of the rotational energy (in kJ/mol). (c) Size of the largest fragment.

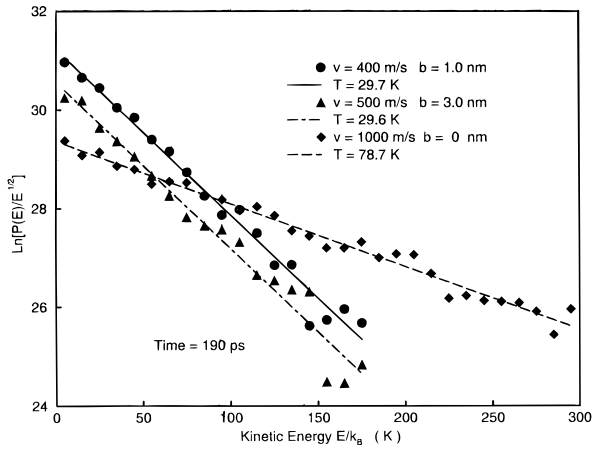

Figure 3. Vibrational kinetic energy distributions for the same collisions as presented in Figures 1 and 2 at the collision time 190 ps. The points are computed using eq 5, and the lines are obtained by a least-squares method. Note that linearity indicates a thermal distribution.

presented in Figure 2. The results shown in Figures 1−3 correspond to three trajectories representing the different collision categories identified. Details of the dynamics, like the fragmentation pattern, do differ between equivalent collisions (i.e., with the same v_{rel} and b but different orientation) whereas the process of energy transfer is much less affected by the precise initial conditions. This is revealed by the smooth curves obtained when the vibrational and rotational excitations are plotted as a function of the impact parameter, as discussed below.

In Figure 4, the final vibrational kinetic temperature is plotted as a function of the impact parameter. The vibrational excitation decreases with increasing impact parameter, and for a given impact parameter we observe that the vibrational excitation is strongly correlated with the collision energy. In Figure 5, the

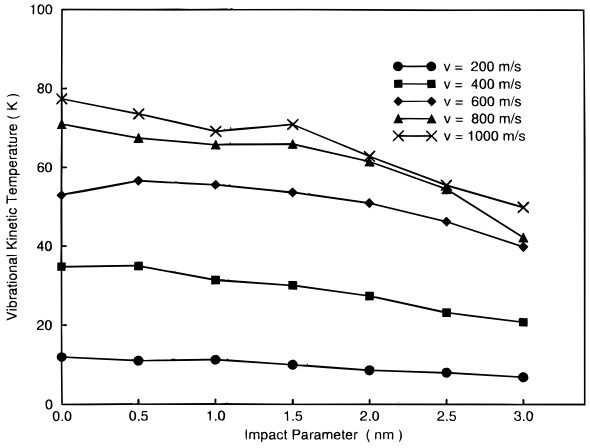

Figure 4. Final vibrational kinetic temperature of the largest fragment as a function of the impact parameter is presented for different collision velocities, from 200 to 1000 m/s. The temperature is computed using eq 3.

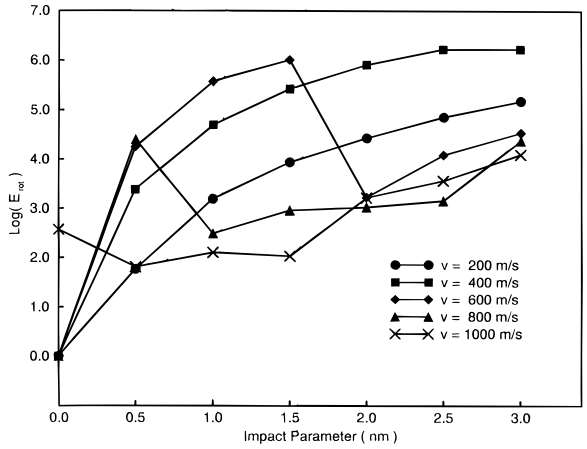

Figure 5. Final rotational energy for the largest fragment as a function of the impact parameter are presented for different translational velocities, from 200 to 1000 m/s. Note the logarithmic energy scale (the unit of energy is kJ/mol).

final rotational energy is plotted as a function of the impact parameter for different velocities. For the pure coalescence collision curves (v_{rel} = 200 or 400 m/s), the final rotational energy increases monotonically with increasing impact parameter. When the relative velocity is further increased (600 or 800 m/s), stretching separation sets in at a sufficiently high b value, and there is a drop in the final rotational excitation. This is due to the fact that the largest fragment only consists of about half of the total number of atoms so that the total rotational energy is splitted into three parts: rotational energy for the two largest fragments as well as relative translational energy. For the highest relative velocity, v_{rel} = 1000 m/s, rotational energy excitation is less pronounced due to severe fragmentation, in which most of the energy is transferred into the relative translational motion among many fragments.

3.3. Fragment Distributions. The fragment distribution was analyzed at the end of each trajectory. Clearly, the fragmentation depends strongly on the collision energy and the impact parameter. For coalescence collisions, there is only one large fragment consisting of almost all atoms. Fragment distributions for v_{rel} = 600 m/s, b = 2 nm (stretching separation collision) and v_{rel} = 1000 m/s, b = 0 (shattering collision) are presented in Figure 6a,b. For the stretching separation collision fragments have a size either around 1000 atoms or below 25 atoms. The number of atoms in the two large fragments is decreased when a higher translational velocity is employed. Though the

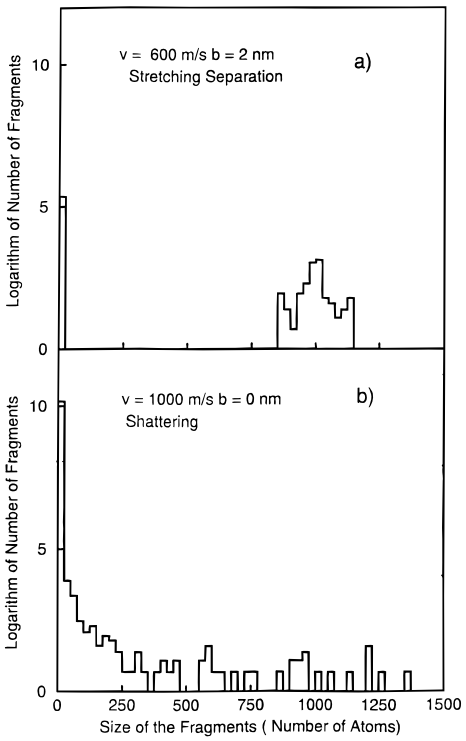

Figure 6. Fragmentation distributions. The analysis is based on 50 trajectories for each distribution. The width of each bin is 25 atoms, and the number of fragments is presented on a logarithmic scale.

fragmentation in the shattering collision is dominated by formation of smaller sized fragments with $N < 25$, there is a certain probability to find a fragment in the range from 25 to 1600.

3.4. Statistical Analysis and Collision Process Overview. Because these calculations are rather time-consuming, single trajectories were employed for most of the initial b and v_{rel}. To check the statistical reliability, 10 trajectories were computed at conditions that are at the boundary between the different types of collisions. The only difference in initial conditions for 10 such trajectories is the rotational orientation of the clusters. The results for the largest fragment in these calculations are presented in Table 1. When there are two or more different collision processes involved, the uncertainty in fragment size is large while the standard deviation of the vibrational temperature is almost independent of the different collision conditions.

Figure 7 presents an overview of the three scattering channels as a function of v_{rel} and b. This type of diagram is adopted from the study of droplet−droplet collisions.[20,31] For a given value of b, the critical velocity v_c defining the region of coalescence collisions is estimated from the data in Table 1 requiring that the probability of coalescence should equal 0.5. When necessary, a linear interpolation was used to obtain v_c. The shattering region is less well defined due to mixing of all three processes. Figure 7 shows that coalescence collisions occur in the low-velocity region, shattering collisions occur at high velocity and small impact parameters, and stretching separation collisions occur at relatively high velocity and large impact parameters.

4. Discussion

We will in the following first relate our results to the limited number of earlier studies of cluster collision processes. We will then compare with experimental and theoretical studies of water droplet collisions.

TABLE 1: Averages over 10 Trajectories Are Presented for Collisions Occurring nearby the Border Lines in Figure 7[a]

b, nm	v_{rel}, m/s	$\langle T_{vib}\rangle \pm \delta T$, K	$\langle N\rangle \pm \delta N$	C	S	Sh
0.0	800	71.5 ± 0.6	1810 ± 4	10	0	0
0.0	900	74.6 ± 0.6	1480 ± 33	2	0	8
0.0	1000	74.9 ± 0.7	1005 ± 76	0	0	10
0.5	800	70.1 ± 0.6	1827 ± 6	10	0	0
0.5	900	73.1 ± 0.8	1836 ± 89	2	0	8
1.0	700	58.8 ± 0.3	1971 ± 2	10	0	0
1.0	800	67.8 ± 0.4	1571 ± 129	6	3	1
1.0	900	72.0 ± 0.8	957 ± 34	0	4	6
1.5	600	52.7 ± 0.3	1996 ± 1	10	0	0
1.5	700	57.2 ± 0.5	1309 ± 145	3	7	0
1.5	800	65.6 ± 0.4	1020 ± 16	0	10	0
2.0	500	37.3 ± 0.3	2000 ± 0	10	0	0
2.0	600	51.4 ± 0.4	1045 ± 7	0	10	0
2.5	400	22.5 ± 0.2	2000 ± 0	10	0	0
2.5	500	35.8 ± 0.5	1124 ± 97	1	9	0
3.0	300	11.6 ± 0.1	2000 ± 10	10	0	0
3.0	400	20.7 ± 0.3	1416 ± 159	5	5	0
3.0	500	30.4 ± 0.4	1020 ± 4	0	10	0
3.5	300	9.4 ± 0.0	2000 ± 0	10	0	0
3.5	400	15.7 ± 0.3	1001 ± 2	0	10	0
4.0	200	3.9 ± 0.0	2000 ± 0	10	0	0
4.0	300	6.2 ± 0.3	1003 ± 1	0	10	0

[a] $\langle T_{vib}\rangle$ is the average temperature of vibration for the largest fragment at the end of the trajectory; $<N>$ denotes the average number of atoms in the largest fragment; C, S, and Sh denote coalescence, stretching separation, and shattering collisions, respectively; δ is the standard deviation.

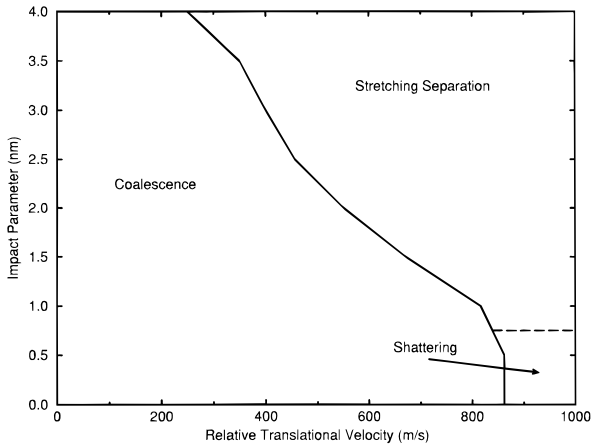

Figure 7. Overview of the collision processes for the range of v_{rel} from 100 to 1000 m/s and b from 0 to 4 nm. The solid line indicates that there is 50% probability for coalescence. The dashed line approximately defines the boundary between stretching separation and shattering.

4.1. Cluster Collision Processes. The general behavior found for Ar cluster−cluster collisions in this study is comparable to the results obtained by Greenspan and Heath[1] for collisions between water-like clusters. The energy scale is shifted due to the higher stability of the water clusters, and we cannot directly compare the energy transfer characteristics for the two systems since no detailed information was given by Greenspan and Heath. Experimental investigations have been carried out on two processes that are related to the present work: the formation of cluster beams and cluster collisions with solid surfaces. Cluster beams can be formed by free jet expansion of a high-pressure gas into vacuum. During gas expansion at relatively low gas densities, small clusters are formed by adsorption of single atoms or molecules on small condensation nuclei. When the gas density is increased, the relative concentration of monomers rapidly decreases, and large clusters are instead formed by cluster−cluster collisions.[32] The relative velocity in these collisions should be quite low due to

the temperature drop during the expansion, and coalescence collisions will therefore dominate, as indicated by Figure 7. Cluster collisions at higher relative velocities could be studied by crossed molecular beam experiments, but we know of no published study of this type. On the other hand, cluster collisions with solid surfaces have received considerable attention recently,[9−17] and the surface impact processes are closely related to the behavior in cluster−cluster collisions. We have carried out trajectory calculations for argon,[9,11,12] mixed argon and neon,[10] and water cluster[13] scattering from solid surfaces. At low velocities, surface impact leads to rapid thermalization and disintegration through evaporation, similar to the results seen for cluster−cluster collisions. At higher impact velocities, shock waves may be formed inside the cluster, which may open up new paths for chemical reactions.[16−18] We have made no detailed study of this phenomenon for cluster−cluster collisions, but similar conditions prevail during head-on collisions with high velocities, i.e., in the shattering regime. It is of interest to compare our head-on collision of two identical clusters with the collision between a Ar_nNe_m ($n + m = 111, 859$) cluster and a rigid surface as in ref 10. The collision energy per atom in the present cluster−cluster case is given by $mv_{rel}^2/8$, where m is the mass of the Ar atom. Comparing this to the energy per atom in the cluster−surface case, $mv^2/2$, one finds that the same collision energy is obtained if $v_{rel} = 2v$. In ref 10, the ejection of fast (nonthermal) atoms was observed to set in at collision velocities of 450 m/s. This is in good agreement with the current study, where we find a transition velocity of 800−900 m/s between coalescence and shattering for head-on collisions. This agreement reflects the fact that the repulsive Ar−Ar interaction plays a dominant role in the shattering regime, where the attractive interaction is comparably weak.

4.2. Comparison with Studies of Water Drop Collisions. Ashgriz and Poo[31] carried out collision experiments with water drops in the micrometer to millimeter size range. Two drop streams collided with relative velocities of 1−20 m/s, and single collisions were followed with high-speed video recording. Two different types of separating collisions were identified, reflexive and stretching separations, and they determined the boundaries between these processes and coalescence. Reflexive separation was found for near head-on collisions with high velocity while stretching separation occurred for large impact parameters. It is far from obvious that our small argon clusters with a diameter of only 4.5 nm should behave in a way that resembles the results for water drops. Nevertheless, we conclude that the coalescence and stretching separation phenomena qualitatively resemble the results using macroscopic drops. We do not observe the reflexive separation collisions that may occur when two large drops collide with a small impact parameter. In the hydrodynamic (macroscopic) picture, the degree of dissipation of fluid kinetic energy to heat depends on the viscosity, velocity gradients within the fluid, and the time available for dissipation to act. For nanometer-sized clusters colliding head-on at several hundreds of m/s, it is obvious that velocity gradients within the clusters will be huge during the early phase of a collision, as well as the corresponding "viscous forces". Kinetic energy is therefore effectively transformed to random vibrational motion, resulting in internal temperature increase. This may be one reason for the absence of the reflexive separation process in our simulations. The argon cluster is also rather fragile compared to a corresponding water cluster, and we believe that this also decreases the likelihood to observe the phenomenon. The reflexive separation should probably become observable if the argon cluster size was considerably increased.

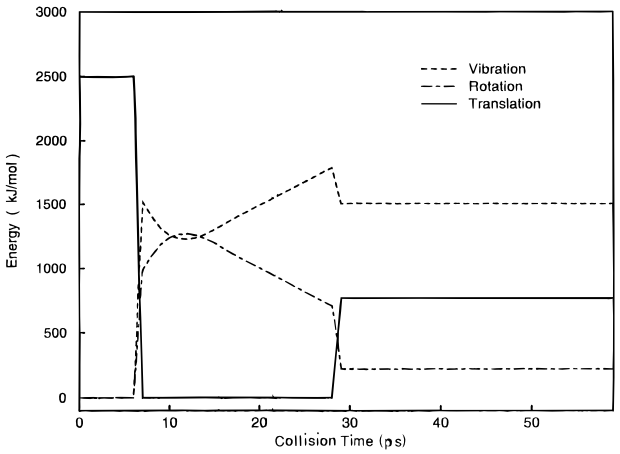

Figure 8. Time-resolved diagram of energy transfer among the vibrational, rotational, and translational degrees of freedom is presented for a collision at $v_{rel} = 500$ m/s and $b = 3$ nm. The vibrational and rotational energies are computed for both clusters when they are coalesced and as the sum of two clusters when they are separated. The translational energy is computed as the relative translational energy between the two clusters. Note that the sum of vibrational, rotational, and translational energies is conserved by this definition.

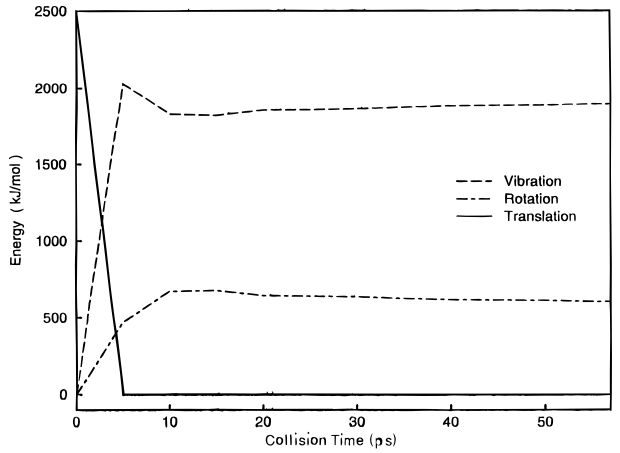

Figure 9. Same as Figure 8 but for $b = 2$ nm.

To further clarify the energy redistribution taking place during collisions with large impact parameters, we have studied the time dependence of different energy terms for a large number of trajectories. A typical trajectory for a relatively large impact parameter of 3 nm is shown in Figure 8. The initial relative velocity of 500 m/s corresponds to a translational energy of 2500 kJ/mol. When the two clusters collide after 6 ps, energy is first transferred to rotational energy of the complex and vibrational energy in the form of kinetic energy. The rotational energy then rapidly reaches a maximum and starts to decrease as the complex stretches. The stretching motion of the complex will turn up as vibrational energy in our analysis, and during this phase some of the rotational energy will also be transferred to heat. The complex finally separates into two large fragments after 28 ps. The final relative translational energy of 770 kJ/mol is comparable to the rotational energy just before the separation. The final total rotational energy of the two clusters is 230 kJ/mol, while the final vibrational energy is 1500 kJ/mol, corresponding to a vibrational temperature of 30 K. Most of the total energy thus ends up in vibrational energy of the cluster, which is only moderately heated due to the very large number of vibrational degrees of freedom. A second trajectory for the same incident velocity but for $b = 2$ nm is shown in Figure 9. This trajectory results in coalescence, as can be seen in Table 1. The initial part of the collision is comparable to

the previous trajectory. The vibrational energy stabilizes at 1900 kJ/mol, while the rotational energy reaches 700 kJ/mol about 10 ps after impact and then only very slowly decreases. The collision complex is in this case more strongly heated already at impact, and too little energy remains for stretching and separation of the complex to occur. Studies of single trajectories also show that the mixing of stretching separation and coalescence collisions for some impact parameters and velocities, seen in Table 1, reflects the influence of detailed impact conditions on the outcome. Using a velocity of 400 m/s and $b = 3$ nm, about 50% end up in each channel. The clusters initially have an internal temperature close to 0 K and some smooth crystal planes on the surface. If two clusters collide with crystal planes directed toward each other, the clusters "bind" more effectively, which leads to coalescence. If the clusters instead make contact with an "edge" on the cluster surface, the resulting binding energy is smaller, and stretching separation is likely to result.

By following several trajectories, we have concluded that a complex rotational energy of about 800 kJ/mol is required for stretching separation to occur. A few models have been proposed based on a comparison between the rotational energy and some effective surface energy. Park[33] derived a model where stretching separation was to occur when the angular momentum was balanced by the surface tension in the region of contact between two droplets. In a model proposed by Brazier-Smith et al.,[34] separation occurs if the rotational energy exceeds the surface energy required to re-form the original drops from a coalesced spherical drop. Arkhipov et al.[35] used the minimum potential energy variational principle by equating to zero the first variation of the potential energy of the system in a coordinate system rotating with constant angular velocity. Ashgriz and Poo[31] proposed an alternative model where they divided the colliding drops into two portions. A small portion of the drops come into contact and form a region of interaction. The remaining portion of each drop is unaffected by the collision and tends to continue in the direction of the original trajectory. Separation occurs when the kinetic energy in the remaining part of the drops, plus a fraction of the kinetic energy in the region of interaction, is larger than the surface energy at the region of interaction. Ashgriz and Poo[31] applied all four mentioned models to their experimental results on water droplet collisions and found good agreement using their own model and the model by Brazier-Smith et al.[34]

To illustrate the similarities between nanometer-sized clusters and micrometer-sized droplets, we have applied the models by Brazier-Smith et al.[34] and Arkhipov et al.[35] to the argon cluster system. For particles of equal size, the critical impact parameter, b_{critical}, leading to separation is given by the following formula

$$b_{\text{critical}}/d = c(\gamma/\rho d)^{1/2}/v \qquad (6)$$

where γ is the surface tension, ρ is the density, and d is the particle diameter. The constant c is different for the two models. Brazier-Smith et al. found $c = 2.50$ whereas Arkhipov et al. have $c = 3.47$. In the present study the diameter of the initial Ar_{1000} cluster was estimated by adding σ to $2R_{\text{max}}$, where R_{max} is the distance from the center of mass to the most distant atom. Using the resulting diameter of 4.46 nm, the density of the initial cluster becomes 1430 kg/m^3. The surface tension is difficult to obtain in our case due to the extremely low initial temperature. Also, the fact that the temperature may increase over 60 K during the process complicates the choice of γ. Assuming that the cluster is a homogeneous Lennard-Jones "fluid" and approximating the pair distribution function with a step function,[36] one finds that $\gamma = 0.024$ N/m, which does not seem to be too unrealistic judging from literature data existing down to 85 K.[37] Note that the square root dependence in eq 6 decreases the effect of variations in γ.

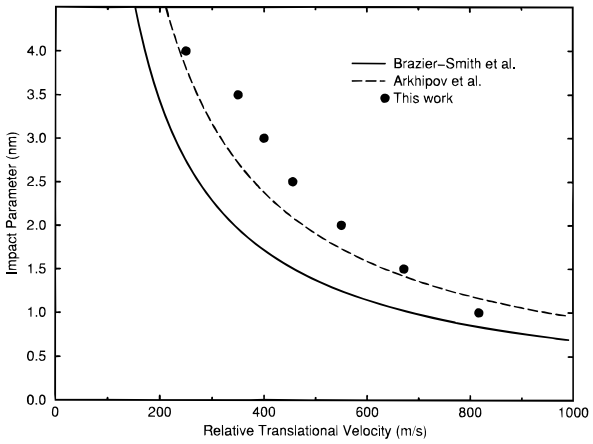

Figure 10. Macroscopic models (eq 6) predicting the critical impact parameter at the transition between coalescence and stretching separation are compared with the present trajectory results.

The model results are in Figure 10 compared with the position of the boundary between coalescence and stretching separation found in the trajectory calculations. The agreement is surprisingly good considering the difference in particle size and conditions for which the models were developed. The use of clusters with an initial temperature above 0 K would probably shift the coalescence boundary to lower velocities. We conclude that the models give at least a qualitative description of both millimeter water droplets and nanometer argon clusters, and this conclusion is therefore likely to hold for the complete range from a few nanometers to millimeters. We also investigated a simple model in which the complex rotational energy is taken as the impact value for two hard spheres. If this rotational energy is to overcome an effective "binding energy" between the clusters, which is assumed to be independent of b and v_{rel}, we note that the same C/v form as in eq 6 is recovered. Further studies are in progress addressing the effects of cluster temperature, cluster size, and composition on the position of the boundary.[21]

5. Conclusion

We conclude that collisions between argon cluster with a diameter of 4.5 nm partially show the same behavior as macroscopic water droplets. Coalescence and stretching separation collisions are observed, and models used for the macroscopic state are concluded to be applicable also to argon cluster collisions.

Shattering collisions can be observed for both clusters and large droplets, while the reflexive separation collisions seen for large water drops were not observed in the calculations.

We conclude that trajectory calculations of cluster−cluster collisions provide an important alternative method for studies of droplet−droplet collisions. Experimental studies are at present limited to the micrometer range. This study shows that trajectory calculations can be carried out with clusters that are sufficiently large for the clusters to obtain "macroscopic" properties. The use of interaction potentials with reasonable accuracy ensures that relevant information can be obtained. Dynamical calculations can therefore be used to test the validity of empirical models in the nanometer range. This has been done in the present study where models predicting the boundary between stretching separation and coalescence have been shown to be at least qualitatively valid down to a few nanometers. This conclusion indicates that when modeling coalescence processes

where cluster−cluster collisions are important, macroscopic models are likely to be valid down to the nanometer size range.

Acknowledgment. This project was supported by the Swedish Natural Science Research Council.

References and Notes

(1) Greenspan, D.; Heath, L. F. *J. Phys. D: Appl. Phys.* **1991**, *24*, 2121.
(2) Wyatt, B. *Comput. Math. Applic.* **1994**, *28*, 175.
(3) Schmidt, R.; Seifert, G.; Lutz, H. O. *Phys. Lett. A* **1991**, *158*, 231.
(4) Schmidt, R.; Schulte, J.; Knospe, O.; Seifert, G. *Phys. Lett. A* **1994**, *194*, 101.
(5) Lewerenz, M.; Schilling, B.; Toennies, J. P. *J. Chem. Phys.* **1995**, *102*, 8191.
(6) Mestdagh, J. M.; Bell, A. J.; Berlande, J; Biquard, X.; Gaveau, M. A.; Lallement, A.; Sublemontier, O.; Visticot, J.-P. In *Reaction Dynamics in Clusters and Condensed Phases*; Jortner, J., et al., Eds.; Kluwer Academic Publishers: Dordrecht, 1994; p 101.
(7) Huisken, F.; Stemmler, M. *J. Chem. Phys.* **1993**, *98*, 7680.
(8) Ahmed, M.; Apps, C. J.; Hughes, C.; Whitehead, J. C. *Chem. Phys. Lett.* **1995**, *240*, 216.
(9) Pettersson, J. B. C.; Marković, N. *Chem. Phys. Lett.* **1993**, *201*, 421.
(10) Marković, N.; Pettersson, J. B. C. *J. Chem. Phys.* **1994**, *100*, 3911.
(11) Svanberg, M.; Marković, N.; Pettersson, J. B. C. *Chem. Phys.*, submitted for publication.
(12) Svanberg, M.; Pettersson, J. B. C. *Chem. Phys. Lett.* **1996**, *263*, 661.
(13) Svanberg, M.; Marković, N.; Pettersson, J. B. C. *Chem. Phys.* **1995**, *201*, 473.
(14) Xu, G.-Q.; Bernasek, S. L.; Tully, J. C. *J. Chem. Phys.* **1988**, *88*, 3376.
(15) Xu, G.-Q.; Holland, R. J.; Bernasek, S. L.; Tully, J. C. *J. Chem. Phys.* **1989**, *90*, 3831.
(16) Cleveland, C. L.; Landman, U. *Science* **1992**, *257*, 355.
(17) Even, U.; Schek, I.; Jortner, J. *Chem. Phys. Lett.* **1993**, *202*, 303.
(18) Schek, I.; Jortner, J. *J. Chem. Phys.* **1996**, *104*, 4337.
(19) Schelke, M.; Frohn, A. *J. Aerosol Sci.* **1993**, *24*, S513.
(20) Rieber, M.; Frohn, A. *J. Aerosol Sci.* **1995**, *26*, S929.
(21) Svanberg, M.; Liu, M.; Marković, N.; Pettersson, J. B. C. *J. Chem. Phys.*, to be submitted for publication.
(22) Hirschfelder, J. O.; Curtiss, C. F.; Bird, R. B. *Molecular Theory of Gases and Liquids*; John Wiley: New York, 1954.
(23) Raoult, B.; Farges, J.; De Feraudy, M. F.; Torchet, G. *Z. Phys. D* **1989**, *12*, 85.
(24) Allen, M. P.; Tildesley, D. J. *Computer Simulation of Liquids*, Oxford Science Publications: Oxford, 1989; p 78.
(25) Stillinger, F. H. *J. Chem. Phys.* **1963**, *38*, 1486.
(26) Jellinek, J.; Li, D. H. *Phys. Rev. Lett.* **1989**, *62*, 241.
(27) Li, D. H.; Jellinek, J. *Z. Phys. D: At., Mol. Clusters* **1989**, *12*, 177.
(28) Liu, M.; Sewell, T. D.; Nordholm, S. *Chem. Phys.* **1995**, *199*, 83.
(29) Liu, M.; Davidsson, J.; Nordholm, S. *Chem. Phys.* **1995**, *201*, 121.
(30) Liu, M.; Davidsson, J.; Nordholm, S. *J. Chem. Phys.* **1996**, *104*, 9000.
(31) Ashgriz, N.; Poo, J. Y. *J. Fluid Mech.* **1990**, *221*, 183.
(32) Soler, J. M.; Garcí, N.; Echt, O.; Sattler, K.; Recknagel, E. *Phys. Rev. Lett.* **1982**, *49*, 1857.
(33) Park, R. W. Ph.D. Thesis, University of Wisconsin, 1970; p 577.
(34) Brazier-Smith, P. R.; Jennings, S. G.; Latham, J. *Proc. R. Soc. London* **1972**, *A326*, 393.
(35) Arkhipov, V. A.; Vasenin, I. M.; Trofimov, V. F. Translated from *Zh. Prikl. Mekh. Tekh. Fiz.* **1983**, *3*, 95.
(36) Rowlinson, J. S., Widom, B. *Molecular Theory of Capillarity*; Clarendon: Oxford, 1982; p 92.
(37) Rowlinson, J. S.; Widom, B. *Molecular Theory of Capillarity*; Clarendon: Oxford, 1982; p 184.